RSC Advances

ROYAL SOCIETY OF CHEMISTRY

www.rsc.org/advances

RSC Advances

COMMUNICATION

Efficient lithium storage from modified vertically aligned carbon nanotubes with open-ends

Received 00th January 20xx,
Accepted 00th January 20xx

DOI: 10.1039/x0xx00000x

www.rsc.org/

Hyun Young Jung,[a,#,*] Sanghyun Hong,[b,#] Ami Yu,[b] Sung Mi Jung,[c] Sun Kyoung Jeoung,[d] and Yung Joon Jung[b,*]

Here we report the use of vertically aligned carbon nanotubes (VA-CNTs) with controlled structure and morphology as an anode material for lithium-ion batteries. The tailored surface structure and open ends morphology of VA-CNT made by ion milling and transfer processes, increases the accessibility of Li ions, and allow Li ions to diffuse inside as well as surface of CNTs through the generated surface defects leading to the significantly improved lithium ion storage capacity compared to as grown, close-ends VA-CNTs. The irreversible discharge capacity of the modified VA-CNTs anode reaches up to 2350 mAh/g at 2C in the first cycle, and the reversible capacity is in the range of 1200 to 557 mAh/g for the 2nd to 20th cycles. The second insertion capacity of the modified CNTs electrode was 4 times higher than the as grown CNTs and 3.2 times higher than what has been reported for the commercial graphite device.

Since launching of lithium-ion batteries (LIB) by Sony Corporation in early 1990,[1] they have been commercially used as one of the most heavily utilized mobile energy sources in a wide variety of portable electronics such as cell phones, laptops, and hybrid automobiles.[2] The battery performance exclusively depends upon the capacity of electrode materials to hold active species of lithium and their reversible charge and discharge.[3-4] The currently used commercial anode of graphite has excellent stability and low cost but could only be intercalated to a maximum of LiC_6 i.e., one lithium for six carbon atoms, leading to a theoretical limit of its specific capacity, 372 mAh/g.[5] To address these issues, other elements that form high lithium content alloys have been explored, such as Si, Sn and Ge.[6] Among those elements, Si is known to have highest theoretical specific capacity (4200 mAh/g), however the large volume change (>400%) during lithiation and delithiation causes pulverization, resulting in capacity loss in a high number of cycles.[7] Therefore, strategies to overcome mechanical failure in anode materials are required for commercial applications.

Recently, there has been continuing global effort to increase the capacity and improve the lifespan of the lithium-ion cell.[8-14] Among the possible candidates to do this, carbon nanotubes (CNTs) have been widely studied as electrode material for LIB since their unique structure and properties such as large surface area, shorter Li-conduction distance, high electrical conductivity and tensile strength make them well suited as a critical component in novel anode material for enhanced lithium storage.[15-16] The capacity of CNTs results from intercalation of Li ions between the graphite layers and in the interstitial sites of close-packed CNT bundles.[17] Overall, the theoretical calculations suggest that reversible capacities exceeding a LiC_2 stoichiometry (>1116 mAh/g) is attainable for CNTs,[18] which represents a dramatic improvement over conventional graphite limits. The reported reversible capacity of CNTs ranges from 300 to 1,000 mAh/g,[19] and is strongly linked to their different morphologies. Particularly vertically aligned CNTs (VA-CNTs) is an ideal candidate to improve the electrochemical performance due to the effective diffusion into stable sites located on the nanotube surface or inside individual nanotubes.[20-23]

Here, we report the electrochemical properties of VA-CNTs where structure and morphology are engineered through the ion milling and nanotube film transfer processes for lithium-ion battery negative electrodes, with the aim to obtain high lithiation capability and better overall performance. The present work also undertakes in order to understand the influence of morphological features and defects on the electrochemical performance. Our surface defect induced open-end VA-CNTs anode has three notable features for the use as the effective electrode material in a lithium-ion battery. First, Li ion diffusion into the interior of the VA-CNTs through the opened ends and sidewall defects generated by ion-milling and nanotube transfer process can shorten the diffusion length of the redox couple and provide rapid electron transport because the energy barrier for Li diffusion through the defects lowers.[24] Second, the alignment of the VA-CNTs in the direction of ion diffusion and their optimized length by controlling CVD time significantly increases the accessibility of the electrode interior to the

[a] Department of Energy Engineering, Gyeongnam National University of Science and Technology, Jinju, Gyeongnam 660-758, South Korea. E-mail: hyjung@gntech.ac.kr
[b] George J. Kostas Research Institute for Homeland Security and Department of Mechanical and Industrial Engineering, Northeastern University, Boston, MA 02115, USA. E-mail: jungy@coe.neu.edu
[c] Department of Electrical Engineering and Computer Science, Massachusetts Institute of Technology, Cambridge, MA 02139, USA.
[d] Automotive Materials Convergence & System R&D Division, Korea Automotive Technology Institute, Chonan, Chungnam 330-912, South Korea
[#] Authors equally contributed.

electrolyte. Finally, the increased active sites for electrochemical Li insertion/extraction dramatically improve the electrochemical performance. As a result, the lithium ion storage capacity of the treated nanotubes by ion milling process is shown to be significantly improved compared to the non-treated case.

Fig. 1a and 1b-c show the optical and scanning electron microscopy (SEM) images of top and side view of as-synthesized CNTs forest. The CNTs are microscopically well aligned with wavy nanostructure. The network nanostructure is periodically rippled due to the nanotube intrinsic defects and bundling and also interconnected with an average inter-bundle spacing of r ≈ 10 nm providing highly dense and large area nanostructured networks for energy storage electrodes. By controlling the growth time during CVD, we first optimized the length of CNTs, 100 µm for the effective diffusion of Li ions, which is an important factor to determine battery behavior. Fig. 1d-g is schematics showing the fabrication process of battery devices using vertically aligned nanotubes anodes. As shown in Fig. 1e, as-grown CNTs forest (Fig. 1d) is transferred upside down to the copper substrate with carbon adhesive layer on the surface. It should be noted that the top section of the as-grown nanotubes has a single-walled nanotube structure with a closed cap, while the bottom section which is the surface of the transferred electrode (Fig. 1e), has relatively an open ended structure.[25] When used as a battery electrode, Li ions can rapidly diffuse through the opened ends of the VA-CNTs. In Fig. 1h, a Raman spectrum of VA-CNTs was obtained with the red laser of wavelength 785 nm. The peaks corresponding to radial breathing mode (RBM) are typically observed at between 150 and 350 cm^{-1} for single-walled CNTs. The corresponding diameters of the nanotube resonating at these frequencies are 1.1 nm to 0.86 nm. In the Raman spectra by 532 nm wavelength in the Fig. 1i, prominent features at 1330 cm^{-1} indicative of the disorder (D) peak usually assigned to the K-point phonons of A_{1g} symmetry typical in polycrystalline graphite, and at 1584 cm^{-1} (G peak), which is common in single graphite crystals and is attributed to the zone centered phonons of E_{2g}^2 symmetry.[26] The bottom side of the VA-CNTs (or the top of Fig. 1e) had defective tip as evidenced by the higher D band intensity (I_D/I_G=0.64, red solid line in Fig. 1i), where the D/G intensity ratio of the top surface of the as-grown CNTs was 0.26 (blue solid line in Fig. 1i). To increase reactive sites for electrochemical lithium insertion/extraction, we have treated VA-CNTs using Ar ion milling (Fig. 1f). The D to G band intensity ratio of the treated VA-CNTs in Raman spectrum was increased to 0.97 (black solid line in Fig. 1i). For the electrochemical battery performance, half cells were assembled using a lithium film as the cathode and VA-CNTs as the anode that were separated by a polymer membrane soaked in a liquid electrolyte solution consisting of 1.0M lithium hexafluorophosphate ($LiPF_6$) in ethylene carbonate (EC)/dimethyl carbonate (DMC) (Fig. 1g).

Fig. 2 shows SEM and transmission electron microscopy (TEM) images of as grown close end VA-CNTs, open-ended VA-CNTs and artificially modified VA-CNTs. The top section of the as-grown nanotubes (Fig. 1d and 2a) has clearly a single-walled CNT structure with a closed cap as shown in Fig. 2b, while the transferred CNT forest (Fig. 1e and 2c) has an open ended structure as shown in Fig. 2d. Moreover, Fig. 2f verifies that the modified CNTs have defective tip and surface, which corresponds to the Raman measurement in Fig. 1i.

Fig. 3a and b exhibit the results of first and second discharge/charge curves in a galvanostatic mode between 0.2 and 2.8 V at 2C for as grown CNTs of 500 µm length and open-ended CNTs electrode with 100 µm optimized length. The first cycle of both CNT electrodes exhibits a plateau in the voltage range between 0.6 and 0.9 V that is designated by the yellow shaded region in Fig. 3a. Such plateau is found in most graphite or CNT based anodes originated from the reduction of the electrolyte and the formation of a solid electrolyte interface (SEI) layer on the

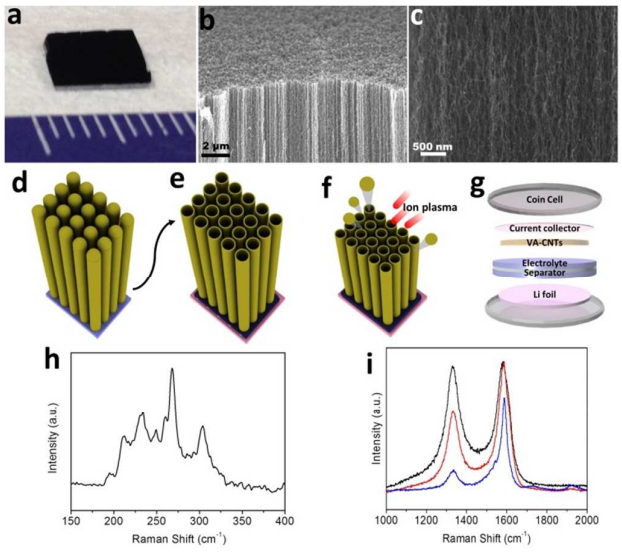

Figure 1 The optical (a) and scanning electron microscopy (SEM) images of top (b) and side view (c) of as-synthesized VA-CNTs forest. (d-g) Schematics of the fabrication process of battery devices; (d) as-grown CNT forest, (e) transferred CNTs on the copper substrate with carbon adhesive layer, (f) modification of CNTs by Ar ion milling, and (g) half cells assembly using a lithium film as the cathode and VA-CNTs as the anode. (h) Radial breathing mode in Raman spectra by 785 nm wavelength of VA-CNTs. (i) D and G band in Raman spectra by 532 nm wavelength of the closed-end (I_D/I_G= 0.26, Blue solid line), open-ended (I_D/I_G= 0.64, Red)and the modified VA-CNTs (I_D/I_G= 0.97, Black).

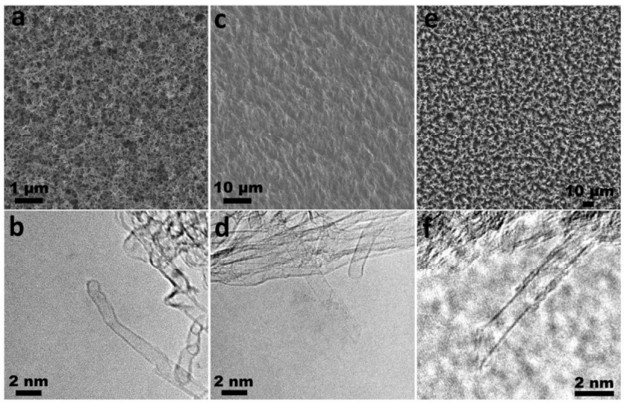

Figure 2 Top surface SEM (a, c, e) and TEM (b, d, f) images of (a-b) as grown close end, (c-d) open-ended, and (e-f) modified open end VA-CNTs.

surface of the electrodes.[27] The capacity of the open-ended CNTs (red solid lines) is larger than that of as grown, close cap CNTs (blue solid lines). This is because the alignment of the short nanotubes in the direction of ion diffusion allows Li ions to more readily access the open nanotube ends, and the surface sites inside and outside the tube offers additional reversible sites for intercalations. Furthermore, once inserted, the lithium ions undergo one-dimensional random walks both inside and outside the tube, and relatively short CNTs allow ions to freely enter and exit. During the first reduction for the open-ended CNTs, a large irreversible capacity of 1980 mAh/g was observed, while a reversible capacity of 607 mAh/g was obtained from the first oxidation. After the formation of SEI in the first cycle, the plateau region vanishes for the second cycle which clearly indicates the irreversible process of SEI formation has been completed, leading to a stable electrolyte–electrode interface.

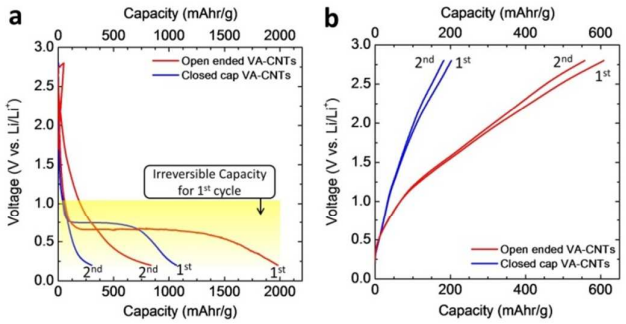

Figure 3 The first and second discharge (a) and charge (b) curves in a galvanostatic mode between 0.2 and 2.8 V at 2C for the closed-cap CNTs (blue solid line) and open-ended CNTs (red solid line).

The specific capacities of the open ended VA-CNTs as function of cycle number are shown in Fig. 4a-b. The second insertion capacity of the open ended CNTs electrode is 920 mAh/g but the capacity decreases with increasing cycles of charge/discharge. The coulombic efficiency in Fig. 4b, a ratio of extraction capacity to the insertion capacity expressed in percent, is reached 98 % after 20th cycles. To characterize the evolution of the kinetic parameters, especially the transport of Li ions within the open ended CNT electrodes, the electrochemical impedance spectroscopy (EIS) was performed (Fig. 4c). The ac impedance spectroscopy was obtained by applying a sine wave of 5mV amplitude over a frequency range of 100 kHz to 0.01 Hz. EIS graphs show one depressed semicircle in the high and intermediate frequency region, which generally corresponds to lithium-ion migration within the SEI layer and the charge transfer through the electrode/electrolyte interface. The 45° line in the low-frequency region shows the typical characteristics of the Warburg impedance,[28] which generally reflects the diffusion process of Li within the bulk electrode. A comparison of the EIS Nyquist complex plots shows that the size of the semicircle drastically decreases after the 2nd discharge cycle. This is because the passive film on the anode surface is destroyed by the de-

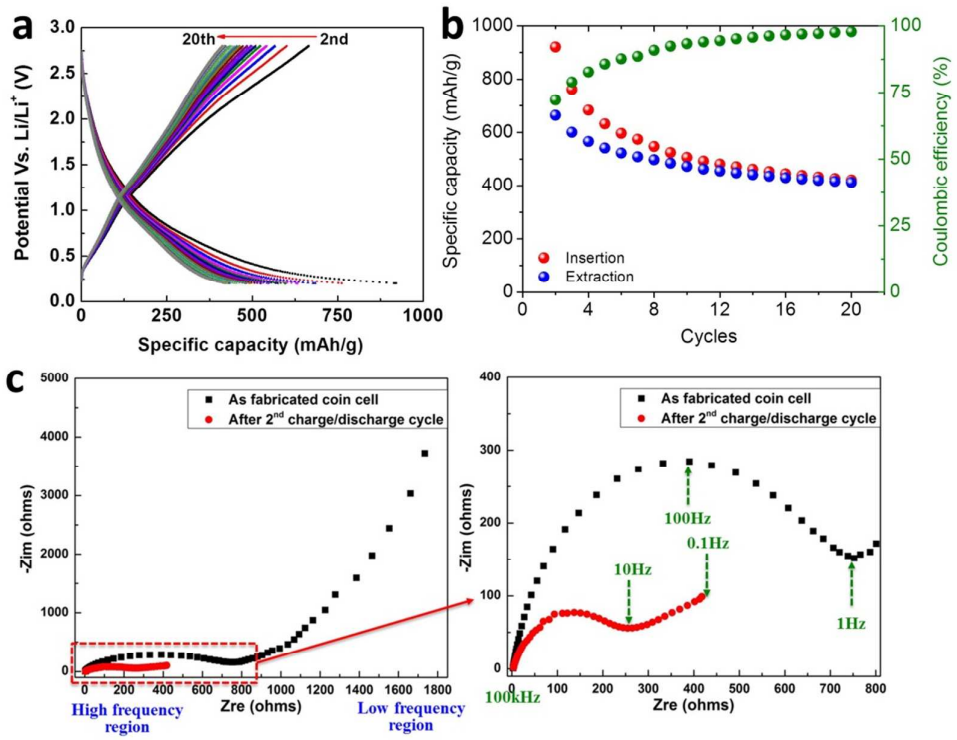

Figure 4 (a) The real time specific capacities of the open-ended VA-CNTs during 2nd to 20th charge/discharge cycles. (b) The specific capacities and coulombic efficiencies as function of cycle number. (c) The electrochemical impedance spectroscopy (EIS) by applying a sine wave of 5mV amplitude over a frequency range of 100 kHz to 0.01Hz.

intercalation of lithium ions from the anode so that the charge-transfer resistance decreases very rapidly.

In addition to the open ended structure of CNTs, defects on the nanotube surface can have better electrochemical performance[24] since the higher presence of defects can provide more available sites for Li ion insertion into the CNTs structure and shorter diffusion distance. Vacancy-type defects created by an Ar ion milling treatment can be thought of as holes on the cylinder of graphene sheets. The presence of these holes allows lithium to better diffuse into and intercalate inside the CNTs (Fig. 5a) resulting in higher irreversible and reversible capacities in the modified CNTs compared to open ended CNTs. Fig. 5b shows the cyclovoltammetry (CV) curves of the open ended and modified CNT electrodes in a coin cell at scan rate of 1 mV/s. The modified open-ended CNTs showed clearly larger current densities in charge and discharge than the open ended CNTs. In the first cycle, an irreversible reduction was observed from the potential around 0.85 V in the cathodic region. This peak is attributed to the decomposition of the solvent and the formation of the SEI on the surface of the CNT electrodes. However, the irreversible reduction almost disappeared after the second cycles, which indicates that the carbon surface was passivated during the first cycle. The cathodic peak at 0 V is associated with Li intercalation and its current density decreased gradually with increasing to 20 cycles. The anodic band at 0.25 V is attributed to the deintercalation of Li stored in sites other than the carbon layers. This anodic peak was particularly noticeable in the modified CNTs (Fig. 5d), indicating Li ions insertion into defect sites residing in the modified CNTs. From 20 cycles to 100 cycles, the CV curves were repeated at the same voltage ranges (Fig. 5c-d). These CV results were correlated with the formation of stage structures of Li-graphite intercalation compounds.

Fig. 6a exhibits the results of first and second discharge/charge curves for the modified open ended VA-CNTs electrodes. The introduction of defects into CNTs shows a further improved reversible capacity as well as irreversible capacity. During the first reduction, a very large irreversible capacity of 2350 mAh/g was observed, while a reversible capacity of 832 mAh/g was obtained from the first oxidation. High irreversible capacity means that lithium ions are essentially consumed by the first cycle and amount of defects also causes a larger amount of lithium ions that are stored on the initial charge cycle to be permanently lost. The second insertion capacity of the modified CNTs electrode was 1200 mAh/g, which was 1.3 times higher than the open ended CNTs and 3.2 times higher than that of the commercial graphite electrode. To understand the capacity stability, the electrodes were subjected to 20 charge/discharge cycles (Fig. 6b-c). The modified CNTs electrodes were approaching towards a stable capacity with coulombic efficiency of 97 % after 8th cycles of charging and discharging operation (Fig. 6c). The capacity gradually decreased with increasing cycles of charge/discharge to be 557 mAh/g at 20th cycles (Fig. 6b-c), which is still higher than that for graphite. Fig. 6d shows the rate capability of the modified CNTs anodes. The reversible capacity of the electrode was around 290, 205, 215, and 405 mAh/g for cycling rate of 4C, 6C, 5.5C, and 3C, sequentially. This indicates that the performance of modified CNTs at high rates was significantly stable by 100th cycles.

Conclusions

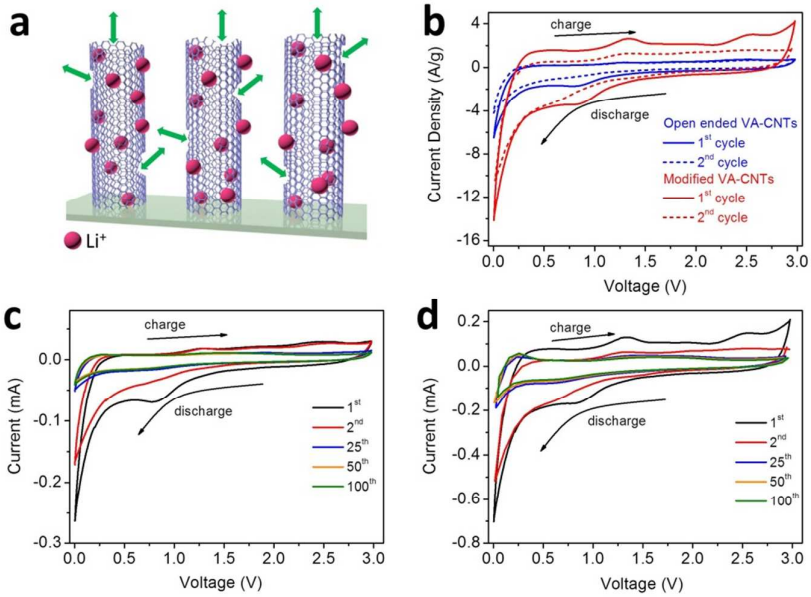

Figure 5 (a) A schematic showing intercalation of Li ions on inside and outside surface of the modified VA-CNTs and diffusion of Li ions through the defective holes (green arrows). (b) The cyclovoltammetry (CV) curves of 1st and 2nd cycles for the open-ended (blue line) and modified CNT (red line) electrodes at scan rate of 1mV/s. The CV curves of the open-ended (c) and modified CNT (d) electrodes by 100 cycles.

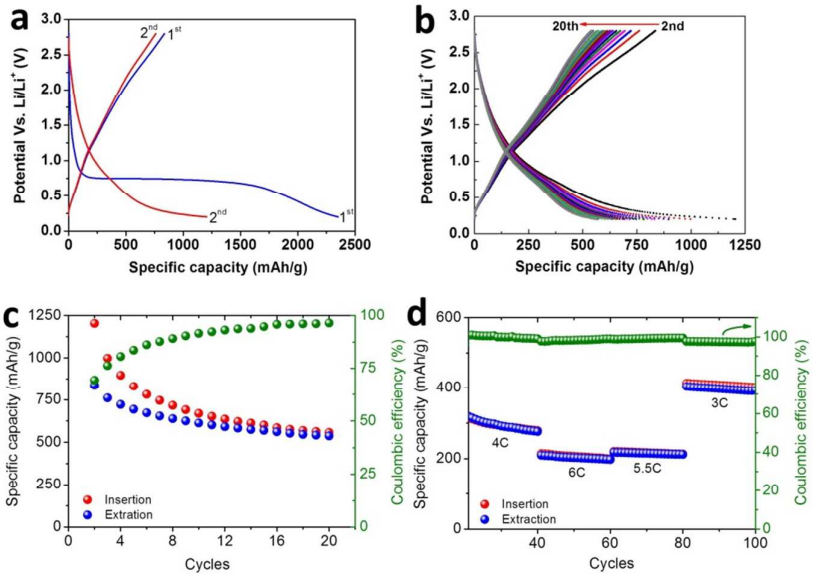

Figure 6 (a) The first and second discharge and charge curves for the modified CNTs in a galvanostatic mode between 0.2 and 2.8 V at 2C. (b) The real time specific capacities during 2nd to 20th charge/discharge cycles. (c) The specific capacity and coulombic efficiency as function of cycle number. (d) The cycling rate capability and efficiency at 4C, 6C, 5.5C, and 3C of the modified CNTs anodes.

In summary, we demonstrated significantly enhanced electrochemical performance of lithium-ion batteries using open ended and artificially modified VA-CNTs electrodes. The VA-CNTs electrodes showed significantly higher rate capabilities compared to graphite. Furthermore, Li ion storage capacity of the open-ended CNTs modified by ion milling process was improved compared to the as grown close end VA-CNTs. The surface defects can provide shorter paths that Li ions can access the internal core of the nanotubes and effective surface sites that the Li ions interact. These results suggest that the VA-CNT electrodes with surface defects can lead to high storage capacities and rate capability as an anode material in lithium-ion batteries.

Experiment section

The VA-CNTs were synthesized on an Al/SiO_2/Si substrate with predeposited cobalt catalyst film (0.4 nm) using 0.5 % C_2H_2 at 800 °C.[29-30] The CNTs were vertically aligned with a height of around 500 and 100 μm (growth rates of ~ 10 μm/min). The etching rate by the Ar ion milling was 0.8~0.9 Å/s under 550 V, 150 mA and 70 degree incident angle.[31] For the battery anodes, all the close-end, open-end and defected open-end CNTs electrodes were formed onto copper substrate with conductive carbon additives. Morphology and structural properties of the prepared anode structures were carefully investigated using a SEM (Zeiss supra 25) and a Raman spectrometer (Jobin Yvon LabRam HR800 with 785 and 532 nm wavelength).

Electrochemical coin cells (half-cells) were assembled using lithium metal and VA-CNTs as the electrodes. Lithium metal foil (99.9 %, Alfa Aesar) was used as the cathode. The electrodes were separated by a Celgard 2500 battery membrane soaked in a liquid electrolyte solution consisting of 1.0M lithium hexafluorophosphate ($LiPF_6$) in ethylene carbonate (EC)/dimethyl carbonate (DMC) (1:1, volume ratio) (Aldrich) solution. CR2032 coin cells were assembled in an argon-filled glove box where the oxygen and moisture content were both maintained below 0.1 ppm.

Electrochemical characterization and electrochemical impedance spectroscopy (EIS) for the anodic materials were carried out by Potentiostat at room temperature. The cells were galvanostatically charged and discharged with cut-off potentials of 2.8 and 0.2 V. Cycling rates were calculated based on the theoretical capacity of graphite, and 1 C corresponds to a specific current of 372 mA/g for the active materials. Before each EIS measurement, the cell was held at the designated potential until the current fell below 0.372 mA/g. The amplitude of the AC signal applied to the electrodes was 5 mV and the frequency was varied from 100k to 0.01 Hz.

Acknowledgements

The authors acknowledge the financial support from National Science Foundation-DMEREF (1434824), US Army under grant W911NF-10-2-0098, subaward 15-215456-03-00, and Technology Innovation Program (10050481) funded by the Ministry of Trade, industry & Energy (MI, Korea)

References

1 T. Nagaura, and K. Tozawa, *Porg. Batteries Sol. Cells.,* 1990, **9**, 209.
2 M. Armand and J.-M. Tarascon, *Nature*, 2008, **451**, 652.

3 H. Zhang, G. Cao and Y. Yang, *Energy Environ. Sci.,* 2009, **2**, 932.
4 K. Kang, Y. S. Meng, J. Breger, C. P. Grey and G. Ceder, *Science*, 2006, **311**, 977.
5 M. Mohri, N. Yanagisawa, Y. Tajima, H. Tanaka, T. Mitate, S. Nakajima, M. Yoshida, Y. Yoshimoto, T. Suzuki and H. Wada, *J. Power Sources*, 1989, **26**, 545.
6 D. Larcher, S. Beattie, M. Morcrette, K. Edstrom, J.-C. Jumas and J.-M. Tarascon, *J. Mater. Chem.,* 2007, **17**, 3759.
7 U. Kasavajjula, C. Wang and A. J. Appleby, *J. Power Sources*, 2007, **163**, 1003.
8 Y. Fan, Q. Zhang, C. Lu, Q. Xiao, X. Wang and B. K. Tay, *Nanoscale*, 2013, **5**, 1503.
9 L. Ji, Z. Lin, M. Alcoutlabi and X. Zhang, *Energy Environ. Sci.,* 2011, **4**, 2682.
10 J.-M. Tarascon and M. Armand, *Nature*, 2001, **414**, 359.
11 J. W. Fergus, *J. Power Sources*, 2010, **195**, 939.
12 P. G. Bruce, B. Scrosati and J.-M. Tarascon, *Angew. Chem. Int. Ed.*, 2008, **47**, 2930.
13 B. Kang and G. Ceder, *Nature*, 2009, **458**, 190.
14 V. Etacheri, R. Marom, R. Elazari, G. Salitra and D. Aurbach, *Enegy Environ. Sci.*, 2011, **4**, 3243.
15 B. J. Landi, M. J. Ganter, C. D. Cress, R. A. Dileo and R. P. Raffaelle, *Energy Environ. Sci.*, 2009, **2**, 638.
16 C. Masarapu, V. Subramanian, H. Zhu and B. Wei, *Adv. Func. Mater.*, 2009, **19**, 1008.
17 C. M. Schauerman, M. J. Ganter, G. Gaustad, C. W. Babbitt, R. P. Raffaelle and B. J. Landi, *J. Mater. Chem.*, 2012, **22**, 12008.
18 J. Zhao, A. Buldum, J. Han and J. P. Lu, *Phys. Rev. Lett.*, 2000, **85**, 1706.
19 C. Casas and W. Li, *J. Power Source,* 2012, **208**, 74.
20 W. Wang and P. N. Kumta, *ACS Nano*, 2010, **4**, 2233.
21 A. Gohier, B. Laik, K.-H. Kim, J.-L. Maurice, J.-P. Pereira-Ramos, C. S. Cojocaru and P. T. Van, *Adv. Mater.*, 2012, **24**, 2592.
22 Y. Zhao, M. Hong, N. B. Mercier, G. Yu, H. C. Choi and H. R. Byon, *Nano Lett.*, 2014, **14**, 1085.
23 H. Zhang, G. Cao, Z. Wang, Y. Yang, Z. Shi and Z. Gu, *Electrochim. Acta*, 2010, **55**, 2873.
24 K. Nishidate and M. Hasegawa, *Phys. Rev. B*, 2005, **71**, 245418.
25 L. Zhu, Y. Sun, D. W. Hess and C.-P. Wong, *Nano Lett.*, 2006, **6**, 243.
26 D. T. Welna, L. Qu, B. E. Taylor, L. Dai and M. F. Durstock, *J. Power Sources*, 2011, **196**, 1455.
27 I. Lahiri, S.-W. Oh, J. Y. Hwang, S. Cho, Y.-K. Sun, R. Banerjee and W. Choi, *ACS Nano*, 2010, **4**, 3440.
28 S. H. Ng, J. Wang, Z. P. Guo, J. Chen, G. X. Wang and H. K. Liu, *Electrochim Acta*, 2005, **51**, 23.
29 M. G. Hahm, Y. Kwon, A. Busnaina and Y. J. Jung, *J. Heat Transfer*, 2011, **133**, 031001.
30 M. G. Hahm, Y. Kwon, E. Lee, C. W. Ahn and Y. J. Jung, *J. Phys. Chem. C*, 2008, **112**, 17143.
31 K. R. Williams, K. Gupta and M. Wasilik, *J. Microelectromech. S.*, 2003, **12**, 761.